ELSEVIER

Journal of Molecular Structure (Theochem) 633 (2003) 35–48

THEO CHEM

www.elsevier.com/locate/theochem

The ring closure of ethylene phosphites is a new P(III)-insertion reaction. A computational study

Jose Kaneti[a,*], Snezhana M. Bakalova[a], Minh Tho Nguyen[b]

[a]*Institute of Organic Chemistry, Bulgarian Academy of Sciences, Acad. G. Bonchev str., Block 9, 1113 Sofia, Bulgaria*
[b]*Department of Chemistry, University of Leuven, Celestijnenlaan 200F, B-3001 Leuven, Belgium*

Received 17 March 2003; revised 31 March 2003; accepted 3 April 2003

Abstract

The observed equilibrium interconversion between open ethylene phosphites and bicyclic spirophosphoranes is recognized as the result of a new insertion reaction of phosphite P(III) into the labile H–O bond of the hydroxyethyl ester, a process more typical to electron deficient species as carbenes or nitrenes, and akin to oxidative additions of transition metals. Energy relationships between species along the reaction path are studied by MO RHF, MP2(full), and MP4SDTQ, as well as DFT calculations, and usually predict 2-hydroxyethyl ethylene phosphites **1** more stable than strained tetraoxo-[10-P-5]-spirophosphoranes **2**, contrary to known experiments. The results of DFT calculations could be referred to underestimation of nondynamic electron correlation in the unfavorable four-electron three-center axial fragment of spirophosphoranes, and thereby spurious prediction of their lower stability. This interpretation of the DFT results is corroborated by CAS SCF vs. MC-QDPT2 calculations.

Keywords: Phosphite; Phosphorane equilibrium; RHF; MP*n*; CAS SCF; DFT calculations

1. Introduction

Bicyclic tetraoxo spiro-[10-P-5]-phosphoranes are important synthetic reagents providing facile routes to numerous biologically active organic phosphate esters such as herbicides, pesticides, plant growth regulators [1–3], as well as phosphorylating agents in nucleotide chemistry [4]. Their reactions are closely related to the transesterification processes of RNA and DNA [4,5], due to the easily, albeit slowly established equilibrium [6] between their half open **1** and cyclic **2** forms, see Scheme 1.

Particularly intriguing is the case of 2-hydroxyethyl phosphite esters **1**, X = : (a lone electron pair) with tri-coordinate phosphorus, which exist in equilibrium with the closed spirophosphorane form **2**, X = H, having five-coordinated phosphorus. The latter reaction has been related recently to phosphate transesterification reactions [5–8] catalyzed by RNA catalysts, ribozymes [9,10]. Spirophosphoranes are good mimics of five-coordinated transition structures and/or intermediates in phosphate ester hydrolysis [11]. There is, however, an important difference

* Corresponding author. Tel: +359-2-9606126 fax.: +359-2-8700225; .
E-mail address: kaneti@orgchm.bas.bg (J. Kaneti).

0166-1280/03/$ - see front matter © 2003 Elsevier B.V. All rights reserved.
doi:10.1016/S0166-1280(03)00279-3

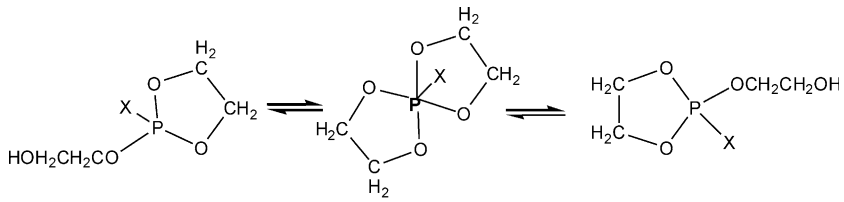

Scheme 1. The phosphite–spirophosphorane equilibrium.

inherent to the latter models of spirophosphoranes: while five-coordinated anionic phosphate transition structures and intermediates are significantly less stable than initial reaction complexes of parent four-coordinated phosphate esters, neutral spirophosphoranes are usually more stable than tri-coordinated phosphite esters. The equilibrium ratio of spirophosphorane **2** vs. ethylene-hydroxyethylphosphite **1** is higher at low temperatures, and is 3:2 in dimethylformamide, respectively, 9:1 in CH_2Cl_2 at room temperature [6,12–14], with thermodynamic parameters of $\Delta G^0 = -0.65$ kcal mol^{-1}, $\Delta H^0 = 2.5 \times$ kcal mol^{-1}, and $\Delta S^0 = 10.6$ entropy units, as determined by ^{1}H NMR [12]. Note, however, that there is no rapid interconversion of **1** to **2** and vice versa at room temperature, and no dynamic NMR process is reported between −60 and 70 °C [12]. Instead, the ligand exchange reaction in a substituted spirophosphorane equilibrates in ca. 20 h at 70 °C [13], thus indicating the typical conditions for the interconversion. Thus, spirophosphorane opening vs. closure reactions are similar in terms of observable rates to e.g. phosphate hydrolysis reactions, known as extremely slow [14].

Kinetic data on intramolecular phosphite to spiro-[10-P-5]-phosphorane conversions usually indicate monomolecular processes [6,12,13,15]. Therefore, the ring closure of hydroxyethyl phosphite esters can certainly be considered an intramolecular reaction. To understand the mentioned experimental results, and thereby add mechanistic insight to the formation and energetics of cyclic intermediates of phosphate hydrolysis, we study theoretically two possible mechanistic alternatives to achieve the equilibrium in the case of hydroxyethyl ethylene phosphite **1**, and tetraoxo spiro-H-phosphorane **2**, namely

(i) a ‘transesterification’ mechanism with attack of the nucleophilic β-hydroxyl oxygen at phosphorus with reaction path involving the transition structure **B**, Fig. 1, and subsequent hydrogen (or proton) O–P migration, and
(ii) a ‘cyclization’ mechanism with phosphine insertion into the O–H bond of the 2′-hydroxyethyl ester **1**, following a reaction path via transition structure **A**.

The commonly assumed driving force to the solvolysis of closed ring ethylene phosphates and phosphates [7,8] to give open hydroxyethyl esters is the enhanced ring strain of five-membered ethylene phosphate, respectively, phosphite or phosphonate esters. The same driving force is considered the reason for the enhanced solvolysis rate of ethylene phosphates and phosphites as related to alkyl esters. One would therefore expect that open chain ethylene phosphates or phosphites would be more stable than strained ring ethylene esters, and even more so compared to spirophosphoranes. The factor opposing the ring strain with the latter compounds could be, e.g. the accumulation of electronegative oxygen atoms around phosphorus. However, while PF_5 has indeed the stabilized trigonal bipyramidal structure, the same ruling is unclear in the case of four (as is the case with spirophosphorane **2**; the fifth substituent is a H) or five oxygen substituents. Therefore, along with the two interconversion mechanisms mentioned above, involving the transition structures **A** and **B**, Fig. 1, we also examine the relative stabilities of all phosphorus species involved in these reactions by ab initio MO RHF, MP2, and MP4, and multiconfigurational MCSCF and MC-QDPT2, as well as by DFT calculations.

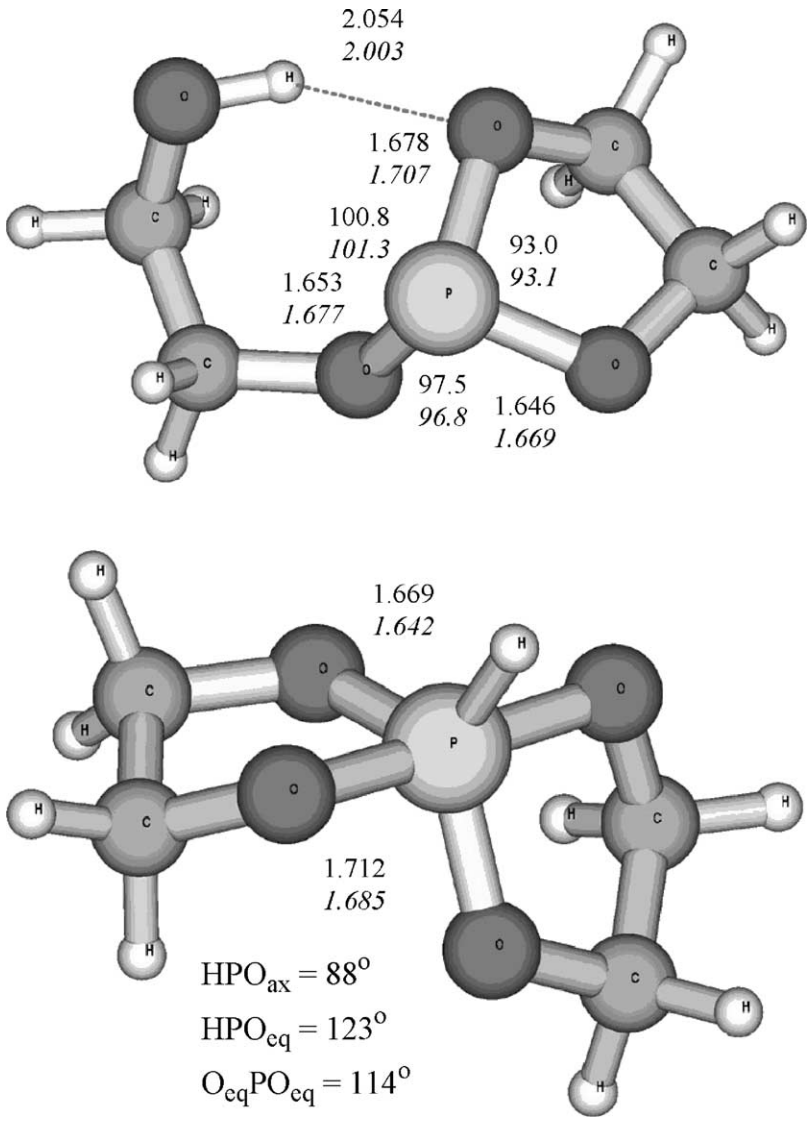

Fig. 1. Theoretical bond lengths and angles, Å and degrees, of 2′-hydroxyethyl- ethylenephosphite **1**, and spiro-[10,P,5]-phosphorane **2**, B3PW91/ 6-311G**, with the MP2(full)/6-311G** values in italic.

2. Computational details

Theoretical relative energies of all species, represented on Scheme 1 and Fig. 1, are studied using several gaussian basis sets, starting with the moderate size 6-31 + G* [16], a mixed basis set (hereafter termed as Gen*) with 6-31G functions for C, H, O, and a polarized MC [17] basis set for phosphorus. Next we use the fully polarized triply split valence basis sets 6-311G(d,p) [17], as well as the 6-311++G(d,p). Our highest is another mixed basis set, consisting of cc-pVTZ [18] on P, and 6-311G** on the remaining atoms, hereafter denoted as Gen** to estimate the basis set dependence of calculated relative energies of studied phosphorus species. The effects of dynamic electron correlation are systematically evaluated by MP2(fc) and MP2(full) geometry optimization [19], and by single

Table 1
Calculated absolute (a.u) and relative (kcal mol^{-1}) RHF MO energies of species involved in the hydroxyethyl ethylene phosphite—bis-ethylene H-spiro[10-P-5]phosphorane equilibrium

Species	HF/6-31 + G*		HF/6-31 + G* water (CPCM)		HF/Gen*		HF/6-311G**		HF/6-311++G**		HF/Gen**	
	E (a.u)	E_{rel} (kcal mol^{-1})	E (a.u)	E_{rel} (kcal mol^{-1})	E (a.u)	E_{rel} (kcal mol^{-1})	E (a.u)	E_{rel} (kcal mol^{-1})	E (a.u)	E_{rel} (kcal mol^{-1})	E (a.u)	E_{rel} (kcal mol^{-1})
1	−796.92408	0	−796.94485	0	−796.74263	0	−797.05306	0	−797.06523	0	−797.08791	0
TS A	−796.82592	61.6			−796.64036	64.2	−796.95138	63.8	−796.96399	63.5	−796.99218	60.1
TS B	−796.83560	55.5			−796.66327	49.8	−796.96367	56.1	−796.97496	57.1	−796.99509	58.2
2	−796.92089	2.0	−796.94057	2.7	−796.73942	2.0	−797.04561	4.7	−797.05433	6.8	−797.08824	−0.2

point MP4SDTQ [20] calculations at the MP2(full) geometries. DFT geometries and energies are evaluated using a variety of functionals, starting with a generalized gradient GGA functional BP86, including the B88 exchange functional [21] and the P86 correlation functional [22]. In addition, we use several hybrid functionals—the popular B3LYP [23] as well as the combinations B3PW91 [24], and BH and HPW91 [24,25]. These calculations are carried out using GAUSSIAN 98 [26], and NWChem [27]. Solvent effects within the CPCM (COSMO) scheme [28] are evaluated using GAUSSIAN 98. IRC calculations [29], and geometry optimizations at the MP2(full)/6-311G** and CAS SCF/6-311G** [30] (eight electrons in eight active orbitals, 8 × 8) levels, as well as single point 12 × 12 CAS SCF/6-311G** and MC-QDPT2 at the 8 × 8 CAS SCF geometries are done with the aid of GAMESS-US [31]. Details in orbital selection for the CAS [30] are discussed along with the results.

3. Results and discussion

3.1. Stationary structures on the $C_4H_9O_4P$ potential energy surface

Calculated RHF, DFT and MP2 absolute and relative energies are listed in Tables 1,2 and 4. The calculated geometry parameters of the tetraoxo spiro-[10-P-5]-phosphorane *2* closely approach the known X-ray structures of a spiro-[10-P-5]-dioxophosphorane [6] and a spiro-[10-P-5]-tetraoxo phosphorane [15]. The theoretical, Fig. 1, as well as the experimental X-ray structures [6,15] are slightly distorted trigonal bipyramids with a central P atom. The O–P–O fragment of spirophosphorane **2** is predicted almost linear with an angle of ca. 175°, while the experimental value is around 179°. The equatorial O–P–O angle is predicted at ca. 113°, while the experimental value is ca. 121°. The two ethylene bridges, forming the five-membered rings, do not cause distortion of the theoretical structure towards a square pyramid [32], but to the contrary, the fragment O–P–O is slightly bent towards the equatorial hydrogen atom, that is, calculations predict the trigonal bipyramid somewhat distorted towards a tetrahedron with oxygen atoms at the vertices, Fig. 1.

3.2. Interconversion via direct nucleophilic attack of phosphite on the hydroxyl bond

The geometry of the located transition structure **A** for the ring closure of tetraoxo-[10-P-5]-spirophosphorane, Fig. 2, MOLDEN [33], together with its electron density distribution, Fig. 3, indicate that the dominating role in the cyclization process is played by phosphite electron pair insertion into the O–H bond followed by proton abstraction akin to carbene insertions. Note specifically the typical three-membered ring arrangement of P, H, and O atoms with distances of 1.501 Å, P–H, 1.419 Å, O–H, and 2.163 Å, P–O, and the 95.6° P–H–O angle, B3LYP/6-311G**, Fig. 1, **A**. MP2/6-311G** predicts approximately the same geometry. Another characteristic indicating the almost complete proton abstraction by phosphite phosphorus in **TS A** is the natural bond orbital occupancy [34] P–H of 1.929, HF/6-31 + G*, slightly smaller than the NBO occupancy of the P–H bond in P-protonated 2′-hydroxyethyl-ethylene phosphite **1**, 1.961. Charge reorganization from **1** to **2** via **TS A**, Fig. 3, indicates smooth increase of electron density on H moving from the β-hydroxyl group in **1** to phosphorus in **2**. In **TS B** however, the electron density on the migrating H is apparently at a minimum, and H is even closer to a naked proton than in starting **1**. To the contrary, H in the spirophosphorane **2** bears some negative charge.

Thus, the alternative transesterification reaction path for the intramolecular conversion of neutral hydroxyethyl ethylene phosphite **2** via TS **B** is a genuine transphosphinylation, see Figs. 1 and 3. The characteristic geometry parameters of TS **B** are P–O distances of 2.062 and 2.081 Å, O–H distances of 1.073 and 1.368 Å, and O–P–O angle of 66.2°, HF/6-31 + G*. The MP2/6-311G** geometry is roughly the same. Though having lower activation enthalpy,

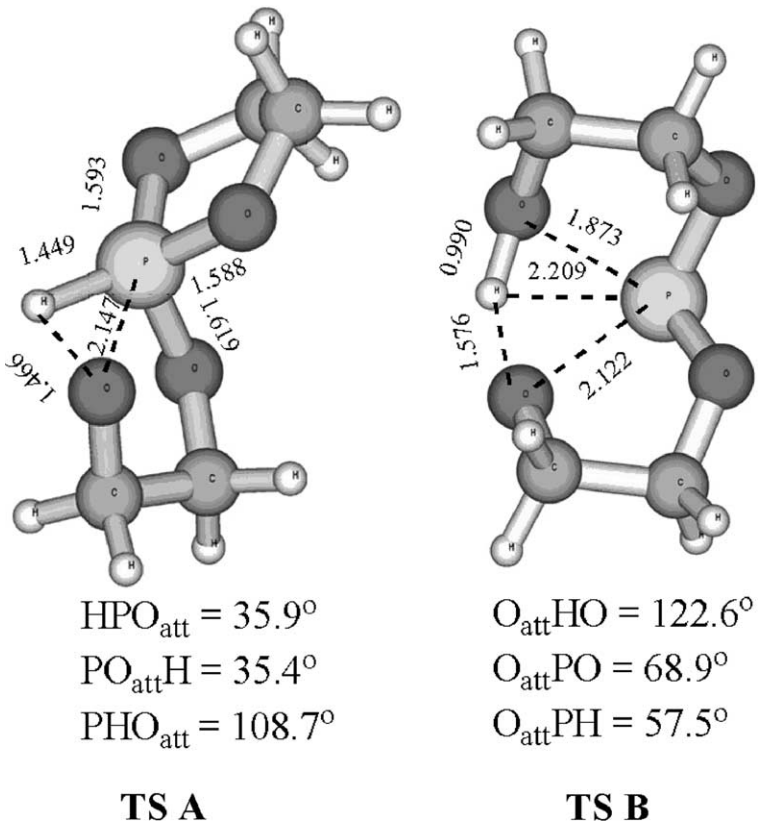

Fig. 2. Optimized transition structures for the two viable mechanisms of phosphite **1** to spirophosphorane **2** interconversion, HF/6-311++G**.

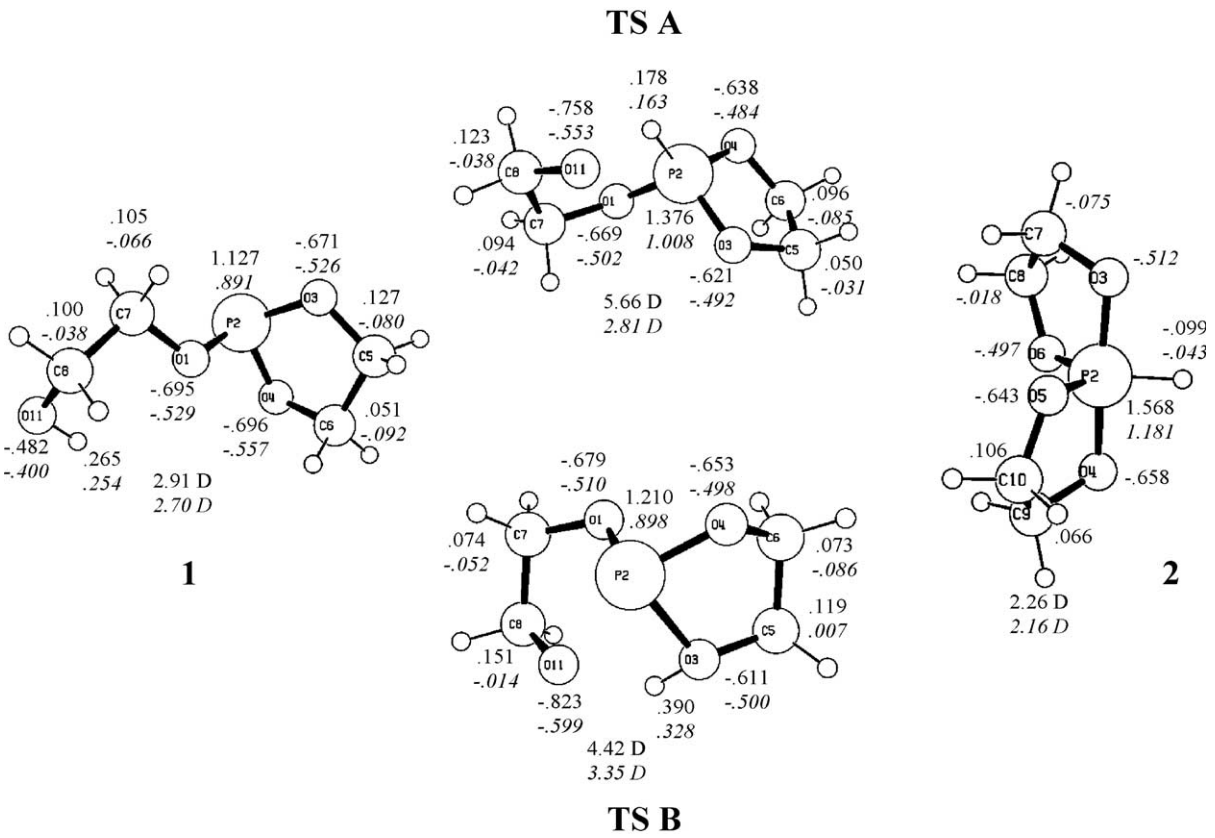

Fig. 3. Mulliken charges and dipole moments of hydroxyethyl ethylenephosphite **1**, 1-H-tetraoxo-[10-P-5]-spirophosphorane **2**, their interconnecting **TS A**, and the transphosphorylation **TS B**, RHF/6-311G** and B3PW91/6-311G**.

the intramolecular transphosphinylation can be considered a side process to the ring closure of the hydroxyethyl phosphite ester **1** into the spirophosphorane **2**, which accumulates during the reaction being the lowest possible minimum [4,12,13]. The located unsymmetrical transition structure **B** represents the conversion path for the phosphite ester into its symmetrically opposite counterpart with a single ring. We confirm this also by MP2/6-311G(d,p) intrinsic reaction coordinate, IRC [29], calculations for the two transition structures **A** and **B**, shown in Fig. 2.

3.3. Interconversion via transesterification and symmetry considerations

Tetraoxo-[10-P-5]-spirophosphorane **2** has an almost perfect trigonal-bipyramidal structure of symmetry C_2, Fig. 1, with the symmetry axis coinciding with the P–H bond. Indeed, there are three (MP2) or two (DFT) other possible structures of low symmetry C_s, **3**, **4**, and **5**, with the symmetry plane containing the P–H bond and bisecting either the space between two ethylenedioxy fragments, Fig. 4, or the mentioned fragments themselves. The latter symmetry orientation, however, could not originate from **TS B**. As shown in Fig. 4, the structures **3**, **4**, and **5** represent the 'movement' of hydrogen along the C_s plane starting from the closest point between 'left and right' **TS B**, and approaching the central phosphorus. The latest of these structures, **5**, has actually an almost square-pyramidal arrangement of substituents at P, with H on the top, and the four oxygen atoms at the base of the pyramid. However, vibrational analyses show that all studied C_s structures possess multiple imaginary frequencies and thus cannot represent any minima on the corresponding potential energy surface,

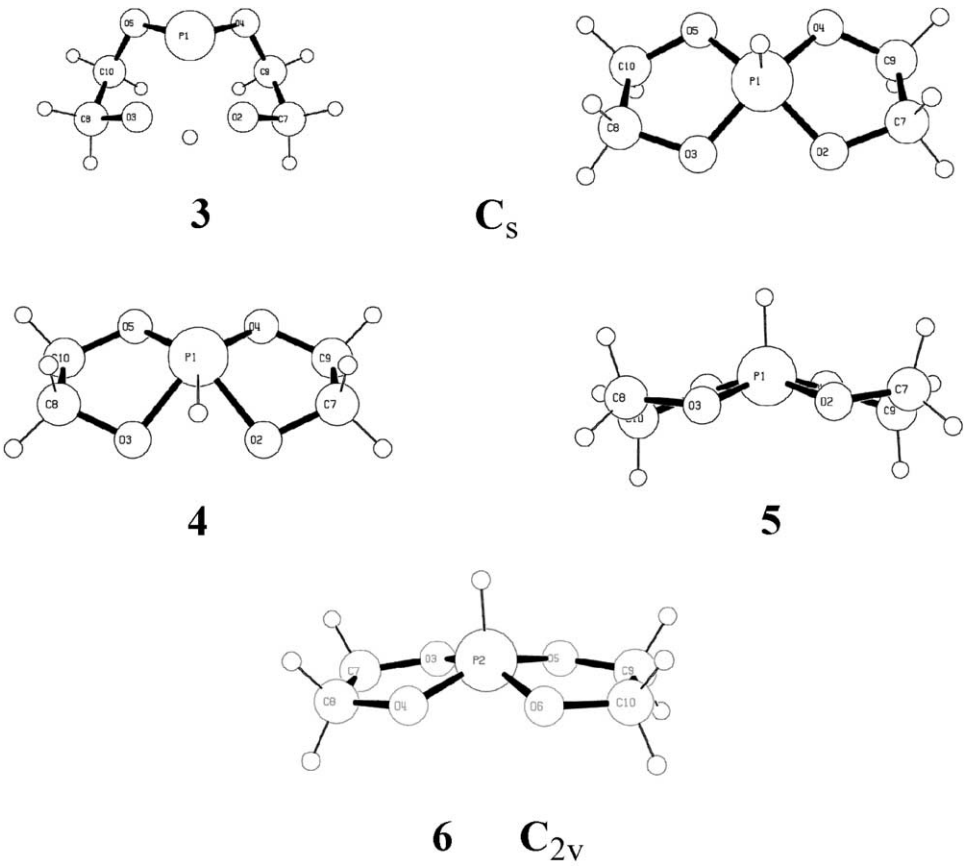

Fig. 4. Symmetry constrained pseudo-stationary species on the spirophosphorane **2** mirror symmetry plane, with two views of the approximately square pyramidal **5**; optimized MP2/6-311G** structures.

PES.The same is valid for the C_{2v} rectangular pyramidal structure **6** with three imaginary frequencies, which is closest to a square-pyramidal species. Table 3 lists the corresponding relative energies of mentioned symmetrical structures along with the number of corresponding imaginary frequencies.

The possible presence of a symmetry plane bisecting the space between the two ethylenedioxy rings formally opens the opportunity for the existence of a symmetry directed interconversion path of open phosphites **1** to spirophosphoranes **2** and vice versa. The obvious candidate for an entry point to such a symmetry determined cross-section of the PES is the hydrogen-bonded 'transesterification' **TS B**: by symmetry, a 'left' and a 'right' **TS B** are equivalent. Thus, a two-dimensional view on the computed energy profiles might create the expectation for a symmetrical intermediate. However, a more detailed consideration of its structure indicates that there are at least two reasons why a symmetry-directed path for the interconversion of **1** to **2** and vice versa is at best of little probability. Mathematically, the crossover point of the multidimensional potential energy surface, PES, on the symmetry plane between the two first order saddle points, the "left" and "right" **TS B**, should be a higher (second, at least) order saddle point. Chemically, as far as the interconversion path between the left and right **TS B** would be the proton shift in a hydrogen bonded system, the crossover point on the symmetry plane should be a local (unidimensional) maximum on the energy profile, hence no intermediate (a true local minimum on the PES) which could be expected on a two-dimensional potential energy surface to virtually represent

a stationary point. Accordingly we conclude that on the true multidimensional PES of hydroxyethyl ethylene phosphite **1**–[10-P-5]-1H-spirophosphorane **2** interconversion any multistep hydrogen migration mechanism is nonexistent. One should add that **TS B** is a true transesterification transition structure, and its transition vector (or imaginary vibrational mode) is not the discussed proton shift either, but rather the P–O bond formation/cleavage.

Calculations of the described symmetry-directed cross-section of the PES are carried out using MP2, as well as B3LYP and B3PW91 at the 6-311G(d,p) basis set level. Included are also other structures with retained symmetry elements. Among these are the aforementioned approximately square-pyramidal forms with C_s, C_2, as well as of C_{2v} symmetry, none of which are local minima, but rather higher other saddle points, see Table 3 and Fig. 4. MP2/IRC calculations starting from located stationary points **3**, **4**, and **5** on the C_s-symmetry plane show that the higher eigenvectors of their corresponding force constant matrices define steepest descent directions, which reduce the symmetry of the corresponding species to C_1. Thus, among the symmetric forms of the conversion hydroxyethyl ethylene phosphite to tetraoxo-[10-P-5]-spirophosphorane there are no hidden isomers or intermediates of the studied half-open to spiro interconversion. In addition, DFT searches along the C_s symmetry plane, starting from the TS B do not locate species **3** and **4** either, while identifying the structure **5** as the transition structure for pseudorotation of the spirophosphorane **2**. No local minima are located in between the other described higher order saddle points on the PES as well, see Table 3.

3.4. A mechanism with direct proton transfer to phosphorus

To rule out the participation of, e.g., external proton sources in the actual liquid phase conversion of open 2′-hydroxyethyl-ethylene phosphites into corresponding spirophosphoranes, we additionally carry out MP2 and DFT 6-31 + G* calculations of protonated species to investigate the possible transformations thereof. Hydroxyethyl-ethylene phosphite **1** has several protonation sites, and the respective number of possible mono-protonated species **7**–**11**, Scheme 2. Calculations of these, the one protonated at phosphorus, as well as the species protonated at a ring oxygen, are carried out to establish their relevance to the studied phosphite to spirophosphorane isomerization, Scheme 2.

B3LYP and MP2 6-31G* searches for saddle point structures show that the P-protonated species cannot undergo ring closure. Protonation of phosphite ester oxygen atoms, too, leads to open intermediates (B3LYP/6-31G*), virtually possessing symmetry elements, or a half-closed species, still a local minimum, owing its relatively stable protonated ethylene phosphite ring to hydrogen bonding with an adjacent oxygen atom, Scheme 2, the species arising from **8** and **11**. All of these intermediates correspond to transphosphinylation reactions (or, more generally, phosphoric ester exchange, transphosphorylation), which is to show again that protonated phosphites cannot undergo ring closure to corresponding spirophosphoranes.

Calculations of deprotonated **1** and **2** in turn produce a single species - the anion of **2**, denoted as **12**, Scheme 2, which we interpret as a strong indication of coordination deficiency, if not electron deficiency, of phosphite P(III), leading to immediate cyclization of the alcoholate anion, corresponding to **1**. The calculated proton affinities of protonated species, Scheme 2, are significantly lower than the value obtained for the phosphoranide [35] anion **12**. The only source of protons in the liquid equilibrium mixture of **1** and **2** are the half-open **1** and the spiro form **2** themselves, as is the case in aprotic solvents as CH_2Cl_2. Thus, we conclude that experimental kinetic data, interpreted as belonging to monomolecular reactions [6,12,13,15], and the present exploration of protonation–deprotonation paths for the conversion of hydroxyethyl ethylene phosphite **1** to spirophosphorane **2** and vice versa in our calculations support unequivocally the characterization of the studied reaction as a phosphorus(III) insertion into the labile O–H bond. What we find is that propensity for insertion reactions can arise from coordination deficiency of a second row atom, P, in the way it arises from electron deficiency of first row atoms (C, N, O) in carbenes, nitrenes, or oxenes. This is supported also by the HOMO electron density map of **TS A**, Fig. 5, which resembles those of transition structures for nucleophilic carbene insertion (as well

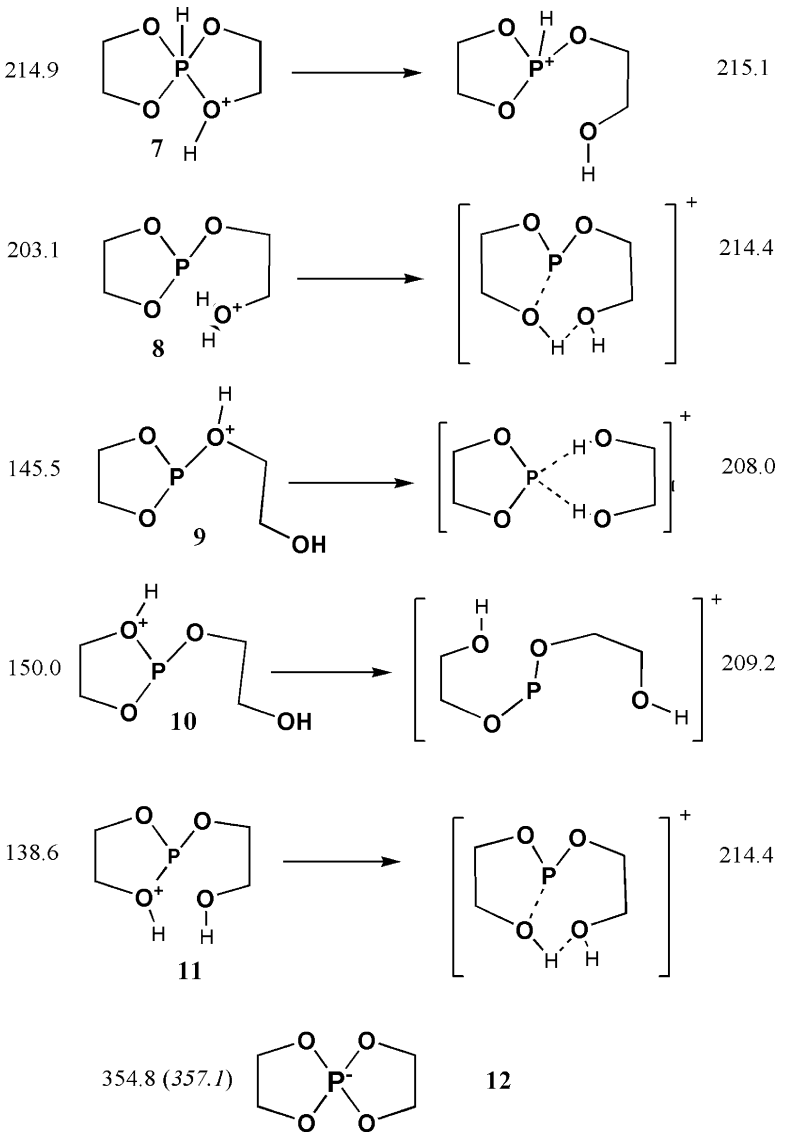

Scheme 2. Protonated and deprotonated species of hydroxyethyl ethylene phosphite **1**, and [10-P-5]-1H-spirophosphorane **2**. Proton affinities are given in kcal/mol (B3LYP/6-31 + G*, see Table 2; for the phosphoranide anion **12** also the B3PW91/6-311++G** value is given in parentheses).

as for the Arbuzov reaction), with the lone electron pair on phosphorus taking the dominant part in the ensuing structural reorganization.

The energy profile of the outlined phosphite **1** - spirophosphorane **2** equilibrium requires first of all reliable evaluation of energies of the involved stable species, **1** and **2**. Calculated optimum RHF and DFT energies with all used basis sets indicate the partially open hydroxyethyl ethylene phosphite **1**, Fig. 1, a little more stable than the closed tetraoxo-[10-P-5]-spirophosphorane **2**, Table 1. However, these results are contrary to experimental determinations of the equilibrium ratio of the open **1** vs. the closed form **2** in solution, 1:9 in CH_2Cl_2 and 2:3 in dimethyl formamide or pyridine. These ratios correspond to ΔG^0, free energy differences, of 0.3–1.5 kcal/mol in

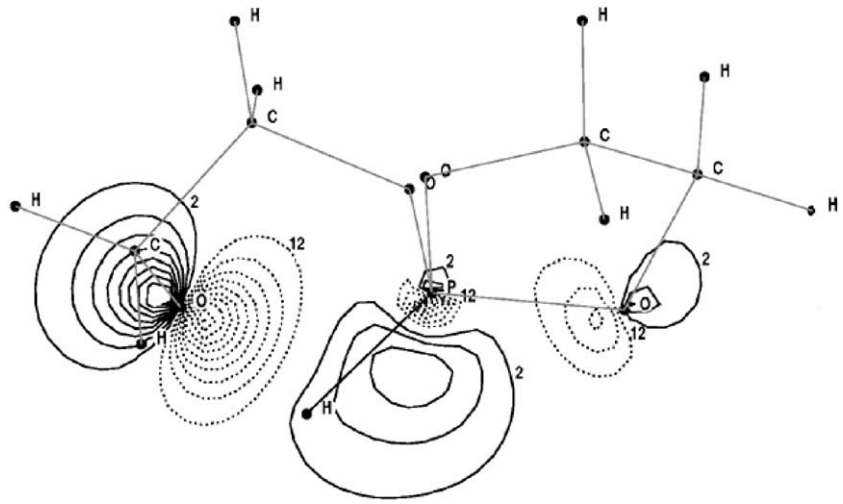

Fig. 5. HOMO electron density map of transition structure **A**, RHF/6-31 + G*.

favor of the spirophosphorane **2**. Limited account for the solvent effect of water using the COSMO model [28] (CPCM in GAUSSIAN 98) at the RHF/6-31 + G* level with no account for electron correlation, see Table 1, predicts the open phosphite **1** more stable than the closed spirophosphorane **2**. These results apparently indicate that the higher stabilities of spirophosphoranes vs. ethylene phosphites are not due to solvent effects. The lower dipole moment, Fig. 3, of spirophosphorane **2** than phosphite **1** accounts correctly for their increased equilibrium ratio in less polar solvents [6,12–14].

Spirophosphorane **2** features the axial three-center O–P–O four-electron fragment, see Fig. 1, which may be expected to pose problems with DFT calculations, due to its similarity to the typical transition structure of S_N2 reactions [36]. However, notwithstanding the analysis of Baerends and coworkers [36], while GGA DFT overstabilizes the S_N2 trigonal–bipyramidal structures with pure carbon p_z-orbitals, our GGA DFT calculations show trigonal–bipyramidal spirophosphorane **2** destabilized with respect to **1**. The participation of d_{z2}-orbitals of phosphorus in the present case instead of p_z orbitals in three-center four-electron S_N2 transition structures, or e.g. s-orbitals in two-center-three-electron bonds, should change the sign of the exchange contribution to the energy difference between **1** and **2** and possibly precondition the result of this calculation by as much as 1.8 kcal/mol in the wrong direction, Table 2. This analysis is corroborated by the DFT finding of a low-lying pseudorotation TS for spirophosphorane 2, only some 8 kcal/mol higher than the stable structure itself, while the corresponding structure on the calculated MP2 PES is as high as ca. 170 kcal/mol and is not a transition structure (the corresponding Hessian FC-matrix has three negative eigenvalues, Table 3), thus indicating a rigid trigonal bipyramidal structure of the spirophosphorane **2** on the computed MP2 energy surface, with no capability for pseudorotation.

On the other hand, calculations using recently developed hybrid functionals, approximating long-range correlation effects using the Coulomb hole approximation for weakly inhomogeneous electron gas on the basis of PW91, e.g. B3PW91 [37,38], furnish improved predictions of the energy relationships and geometries of transition states. Consequently, we chose B3PW91/6-311G** to reevaluate energies of **1** and **2**. Thus we reproduce experimental data somewhat better than with the GGA functional BP86 or with B3LYP by predicting the correct sign of the small energy difference of closed spirophosphorane **2** and open phosphite **1** with the former ca. 3 kcal/mol more stable, Table 2. The calculations with the hybrid combination BHandHPW91/6-311G** [22–24] predict **2** by 2.3 kcal/mol more stable than

Table 2
Theoretical DFT and relative energies of species involved in the phosphite **1** (relative energy 0 kcal/mol)—spirophosphorane **2** equilibrium with various functionals, a.u.

Species	BP86 6-311G**	B3LYP 6-31 + G*	B3LYP 6-311G**	B3PW91 6-311G**	B3PW91 Gen**	BHandHPW91 6-311G**
1	−800.28878	−800.13096	−800.26580	−800.03690	−800.06368	−798.92306
	0.0	0.0	0.0	0.0	0.0	0.0
			−800.26167			
			2.6[a]			
TS **A**	−800.22363	−800.05741	−800.19157	−799.96464	−799.99119	−798.84265
	40.9	46.2	46.6	45.3	45.5	50.5
TS **B**	−800.24491	−800.07372	−800.21168	−799.98213	−800.00473	−798.85817
	27.5	35.9	34.0	34.4	37.0	40.7
2	−800.28598	−800.12921	−800.26259	−800.03666	−800.06846	−798.92665
	1.8	1.2	2.0	0.1	−3.0	−2.3

[a] The *anti*-periplanar (O–C–C–O) conformer of open phosphite **1**

1 at the 6-311G(d,p) basis set level, which is probably an overestimation of the experimentally observed effects.

Less clear are the results of our MP2 and MP4 calculations on open 2′-hydroxyethyl-ethylene phosphite **1** and spiro-[10-P-5]-phosphorane **2**. While the MP*n* perturbation expansion covers systematically the dynamic correlation energy, it is known from analyses by Cremer and coworkers [39] that MP2 somewhat exaggerates electron pair correlation. Accordingly, MP2/6-311G** (and MP2/Gen**) calculations strongly favor spirophosphorane **2** over open phosphite **1**, by 7.7 (respectively 6.9) kcal/mol. The theoretical prediction is reversed in MP4SDTQ/6-311G** calculations, Table 4. Using the parallel to DFT GGA calculations, we relate the result of MP4SDTQ/6-311G**//MP2(full)/6-311G** calculations, which slightly favor (by 1.2 kcal/mol) the open phosphite **1** over spirophosphorane **2**, to negligence of nondynamic electron correlation in MP*n*. Once again, calculations using a more flexible basis set on phosphorus, MP4SDTQ/Gen**//MP2(full)/6-311G**, predict spirophosphorane **2** as favored by 4.8 kcal/mol over open phosphite **1** (−798.732236 a.u., **2**, vs. −798.724523 a.u., **1**). The latter difference should be considered overestimated

Table 3
An energy cross-section for the H-migration along the C_s-symmetry plane of the PES for the hydroxyethyl ethylene phosphite **1**–tetraoxo-[10-P-5]-spiro-phosphorane **2** interconversion. Absolute energies in a.u., relative energies in kcal/mol (E_0 = −798.81259 a.u., MP2/6-311G**; −800.2658, B3LYP/6-311G**; −800.0369, B3PW91/6-311G**)

Species	MP2/6-311G(d,p)		B3LYP/6-311G(d,p)		B3PW91/6-311G(d,p)	
	Energy	Nimag	Energy	Nimag	Energy	Nimag
TS B	−798.75218	*1*	−800.21168	*1*	−799.98213	*1*
	37.9		34.0		34.4	
3	−798.48801	*2*				
	203.2					
4	−798.40660	*2*				
	254.8					
5	−798.54515 (C_2)	*3*	−800.25172	*1*	−800.02611	*1*
	−798.55123 (C_s)	*3*	*8.8*		*6.8*	
	~170					
6	−798.51995 (C_{2v})	*3*	−800.24816	*3*	−800.02238	*3*
	183.6		11.1		9.1	

for the same reason as the former MP4 result, and is indeed higher than found by experiments.

Thus, theoretical energy relationships in studied phosphite–spirophosphorane pairs are very sensitive to both electron correlation and basis set effects, as shown by our DFT calculations with GGA and recent hybrid functionals, as well as by RHF and MP*n* calculations using the Gen* and Gen** basis sets. Provision of an extended set of polarization functions on P, and a polarized basis of moderate size for the rest of atoms in considered molecular species, enables correct (although virtually due to cancellation of errors) predictions of energy relationships even at the RHF/Gen** level of theory, Table 1.

To finally check the interpretation of all factors governing the stability and interconversions of ethylene phosphites **1** to spirophosphoranes **2**, and vice versa, we carry out MC SCF (CAS SCF)/6-311G** [30] calculations of **1**, **2**, and their connecting transition structure, **TS A**, as well as of the transesterification transition structure, **TS B**. The expected result is to verify the trends in energy relationships of open **1** vs. spiro-compound **2**, as well as between the transphosphorylation **TS A** and phosphite insertion **TS A** structures, as deduced from DFT and single configuration MO calculations. Indeed, we cannot even attempt achieving any completeness of the multiconfigurational calculations due to the sheer size of the studied molecular species. Even with a restricted configuration space, the orbital selection is difficult due to the fact that the 10 highest occupied MO's of [10-P-5]-1H-spirophosphorane **2** are oxygen lone pair and σ-CO orbitals, as well as 4 out of the 6 lowest virtual orbitals are σ**-CH orbitals. Thus we are forced to select the active configuration space on purely computational grounds, based on considerations of computing time and available scratch disk space. With the aim to at least find some tendencies in calculated correlation corrections, we test two expansions, denoted hereafter as (8×8), i.e. eight electrons on eight orbitals, and (12×12), i.e. 12 electrons in 12 orbitals, evenly taken as the highest occupied and lowest virtual MO's, see Table 4. The comparison of (8×8) CAS SCF energies, for which geometry optimization is feasible, and dominantly accounting for the nondynamic electron correlation, shows the closed spirophosphorane **2** by as much as 14 kcal/mol more stable than the partially open phosphite **1**. The limited perturbational account for dynamic electron correlation in (8×8) MC-QDPT2 inverses the sign of this energy relationship by almost as much, 9 kcal/mol. Even though the active correlation space accounted for is only eight electrons in eight orbitals, these calculations reveal that nondynamic electron correlation stabilizes η_5-P relative to η_3-P, and vice versa, dynamic correlation brings about stabilization of η_3-P (and possibly η_4-P as well) relative to η_5-P. This deduction is confirmed by the calculated relative energies of **TS A** and **TS B** as well: CAS SCF significantly stabilizes the 'almost η_5-P' **TS A**, with the migrating H almost completely attached to P, and reduces the predicted activation

Table 4
Correlated MO absolute and relative energies of species involved in the phosphite **1** (relative energy 0 kcal/mol)—spirophosphorane **2** equilibrium, a.u. and kcal/mol

Species	MP2-full 6-311G**	SP MP4SDTQ 6-311G**	8 × 8 CAS SCF 6-311G**	SP 8 × 8 MC-QDPT2 6-311G**	SP 12 × 12 CAS SCF 6-311G**	SP 12 × 12 MC-QDPT2 6-311G**
1	−798.81259	−798.65500	−797.11964	−798.55772	−797.19477	−798.55863
	0.0	0.0	0.0	0.0	0.0	0.0
TS **A**	−798.73435	−798.57560	−797.09220	−798.47721	−797.11692	−798.43807
	49.1	49.8	17.2	50.5	48.9	75.7
TS **B**	−798.75218	−798.59460	−797.05003	−798.47797	−797.12438	−798.47885
	37.9	37.9	43.7	50.0	44.2	50.1
2	−798.81405	−798.65316	−797.14220	−798.54271	−797.22993	−798.54355
	−0.9	1.2	−14.2	9.4	−22.0	9.5

MP4SDTQ/6-311G** calculations are done at the MP2(fu)/6-311G** geometry. All MC-QDPT2 (8 × 8), CAS SCF (12 × 12) and MC-QDPT2 (12 × 12)s data are calculated at the corresponding CAS SCF (8 × 8) geometries.

energy of phosphite insertion significantly below the value predicted for the 'almost η_4-P' **TS B**, the transphosphorylation TS. Conversely, MC-QDPT2 over the same correlation space 'restores' the expected relationship between activation energies of **1**–**2** ring closure/opening vs. mirror **1**–**1** conversions within the range of expectations, given by DFT and MP*n* calculations.

The data obtained with the (8 × 8) active configuration space are essentially reproduced at the higher level of electron correlation, using the (12 × 12) active space, with the exception that the (12 × 12) CAS SCF energy gap between **1** and **TS A** is in line with MP*n* results. In fact, the majority of activation energies, calculated here for the mirror transphosphinylation **1**–**1**, with the exception of (8 × 8) MC-QDPT2, are well within the range of theoretical values obtained for phosphate ester reactions [8,14, 40]. The predicted activation energies for the phosphite insertion reaction **1**-**2**, even including the exceptionally low (8 × 8) CAS SCF value, are in turn significantly higher than values obtained for less reactive carbene (e.g. vinylidenes: little, if any, reaction barriers) insertion reactions [41]. We consider the exceptionally low activation energy, predicted by present CAS SCF calculations for **TS A**, already having the 'hypervalent' coordination at P, as one more indication of the importance of balanced account of electron correlation effects in calculations of molecular species and reactions involving atoms with high (or 'hypervalent') coordination numbers.

4. Conclusion

The intramolecular cyclization of partially open phosphite esters, P(III), to spirophosphoranes, P(V), is shown to proceed by a mechanism of phosphite insertion into the labile O–H bond in β-position relative to the PO group. The revealed mechanism is similar to insertion mechanisms of carbenes or nitrenes, and indicates that propensity for insertion reactions can arise from coordination deficiency of P in the manner it arises from electron deficiency of first row elements.

Computationally, the results of the explored various levels of theory underscore the necessity of carefully balanced account of electron correlation effects to properly reproduce the experimental energy relationships in the studied P(III)–P(V) interconversion reaction. Overestimation of second order Møller–Plesset perturbational corrections from electron correlation leads to spurious results at both single and multiconfigurational levels of MO theory. Thus, best correspondence to experimental data is obtained using DFT with the Perdew–Wang correlation functional, and sufficiently large gaussian basis sets, at least 6-311G(d,p), preferably augmented with additional basis functions on phosphorus.

Acknowledgements

The reported MP4 calculations were made by JK while visiting the Lise Meitner—Minerva Center for Computational Quantum Chemistry, Hebrew University, Jerusalem, Israel. We thank professor Sason Shaik for the use of the relevant computational resources.

References

[1] A. Kalir, H.H. Kalir, in: F.R. Hartley (Ed.), The Chemistry of Organophosphorus Compounds, Vol. 4, Wiley, New York, 1996, pp. 767–780.
[2] H.R. Hudson, M. Pianka, Phosphorus, Sulfur, Silicon Relat. Elem. 109–110 (1996) 345–348.
[3] C. Gerber, D. Seebach, Helv. Chim. Acta 74 (1991) 1373–1385. S.A. Beers, C.F. Schwender, D.A. Loughney, E. Malloy, K. Demarest, J. Jordan, Bioorg. Med. Chem. 4 (1996) 1693–1701.
[4] P. Lemmen, W. Richter, B. Werner, R. Karl, R. Stumpf, I. Ugi, Synthesis (1993) 1–10. K. Vercruysse, C. Dejugnat, A. Munoz, G. Etemad-Moghadam, Eur. J. Org. Chem. (2000) 281–289.
[5] E.E. Nifantiev, M.K. Grachev, S.K. Burmistrov, Chem. Rev. 100 (2000) 3755–3799.
[6] S. Kojima, K. Kajiyama, M. Nakamoto, K. Akiba, J. Am. Chem. Soc. 118 (1996) 12866–12867.
[7] D.-M. Perreault, E.V. Anslyn, Angew. Chem., Int. Ed. Engl 36 (1997) 432–450. D.-M. Zhou, K. Taira, Chem. Rev. 98 (1998) 991–1026.
[8] C. Lim, P. Tole, J. Am. Chem. Soc. 114 (1992) 7245–7252. C. Lim, P. Tole, J. Phys. Chem. 96 (1992) 5217–5219.
[9] A.J. Zaug, T.R. Cech, Science 231 (1960) 470–473. G.J. Narlikar, D. Herschalg, Annu. Rev. Biochem. 66 (1997) 19–59.
[10] S.B. Tsokov, R.T. Momtcheva, N.G. Vassilev, J. Kaneti, D.D. Petkov, J. Am. Chem. Soc. 121 (1999) 5103–5107. S.B. Tsokov, PhD Thesis, Bulgarian Acad. Sci., 1998/.

[11] R. Burgada, R. Setton, in: F.R. Hartley (Ed.), The Chemistry of Organophosphorus Compounds, Vol. 3, Wiley, New York, 1994, pp. 185–272. R.R. Holmes, A. Chandrsekaran, O. Day, D.J. Sherlock, P. Sood, T.K. Prakasha, Phophorous, sulfur, Silicon Relat. Elem., 124–125, 1997, pp. 7–22.
[12] A. Munoz, M. Sanches, M. Koenig, R. Wolf, Bull. Soc. Chim. France (1974) 2193.
[13] R. Burgada, Bull. Soc. Chim. Fr. (1975) 407.
[14] Experiment: J.P. Guthrie, J. Am. Chem. Soc. 99 (1977) 3991–4002. A. Radzicka, R. Wolfenden, Science 267 (1995) 90–93. Theory:J. Florian, A. Warshel, J. Phys. Chem. B 102 (1998) 719–734.
[15] C.D. Montgomery, S.J. Rettig, B. Shurmer, Can. J. Chem. 76 (1998) 1060–1063.
[16] R. Ditchfield, W.J. Hehre, J.A. Pople, J. Chem. Phys. 54 (1971) 724–728. W.J. Hehre, R. Ditchfield, J.A. Pople, J. Chem. Phys. 56 (1972) 2257–2261.
[17] R. Krishnan, J.S. Binkley, R. Seeger, J.A. Pople, J. Chem. Phys. 72 (1980) 650–654. A.D. McLean, G.S. Chandler, J. Chem. Phys. 72 (1980) 5639.
[18] T.H. Dunning Jr., J. Chem. Phys. 90 (1989) 1007. D.E. Woon, T.H. Dunning Jr., J. Chem. Phys. 98 (1993) 1358. T.H. Dunning Jr., P.J. Hay, H.F. Schaefer III,Methods in Electronic Structure TheoryPlenum PressNew York (1977) 1–27.
[19] C. Møller, M.S. Plesset, Phys. Rev. 46 (1934) 618. M. Head-Gordon, J.A. Pople, M.J. Frisch, Chem. Phys. Lett. 153 (1988) 503.
[20] R. Krishnan, J.A. Pople, Int. J. Quant. Chem. 14 (1978) 91.
[21] A.D. Becke, Phys. Rev. A 38 (1988) 1098.
[22] J.P. Perdew, Phys. Rev. B 33 (1986) 8822. Erratum:J.P. Perdew, Phys. Rev. B 34 (1986) 7406.
[23] A.D. Becke, J. Chem. Phys. 98 (1993) 5648. C. Lee, W. Yang, R.G. Parr, Phys. Rev. B37 (1988) 785.
[24] J.P. Perdew, K. Burke, Y. Wang, Phys. Rev. B 54 (1996) 16533.
[25] L.A. Curtiss, C. Jones, G.W. Trucks, K. Raghavachari, J.A. Pople, J. Chem. Phys. 93 (1990) 2537.
[26] M.J. Frisch, G.W. Trucks, H.B. Schlegel, G.E. Scuseria, M.A. Robb, J.R. Cheeseman, V.G. Zakrzewski, J.A. Montgomery, Jr., R.E. Stratmann, J.C. Burant, S. Dapprich, J.M. Millam, A.D. Daniels, K.N. Kudin, M.C. Strain, O. Farkas, J. Tomasi, V. Barone, M. Cossi, R. Cammi, B. Mennucci, C. Pomelli, C. Adamo, S. Clifford, J. Ochterski, G.A. Petersson, P.Y. Ayala, Q. Cui, K. Morokuma, D.K. Malick, A.D. Rabuck, K. Raghavachari, J.B. Foresman, J. Cioslowski, J.V. Ortiz, A.G. Baboul, B.B. Stefanov, G. Liu, A. Liashenko, P. Piskorz, I. Komaromi, R. Gomperts, R. L. Martin, D.J. Fox, T. Keith, M.A. Al-Laham, C.Y. Peng, A. Nanayakkara, C. Gonzalez, M. Challacombe, P.M.W. Gill, B. Johnson, W. Chen, M.W. Wong, J.L. Andres, C. Gonzalez, M. Head-Gordon, E.S. Replogle, J.A. Pople, Gaussian 98, Revision A.7, Gaussian Inc., Pittsburgh, PA, 1998.
[27] R.J. Harrison, J.A. Nichols, T.P. Straatsma, M. Dupuis, E.J. Bylaska, G.I. Fann, T.L. Windus, E. Apra, J. Anchell, D. Bernholdt, P. Borowski, T. Clark, D. Clerc, H. Dachsel, B. de Jong, M. Deegan, K. Dyall, D. Elwood, H. Fruchtl, E. Glendenning, M. Gutowski, A. Hess, J. Jaffe, B. Johnson, J. Ju, R. Kendall, R. Kobayashi, R, Kutteh, Z. Lin, R. Littlefield, X. Long, B. Meng, J. Nieplocha, S. Niu, M. Rosing, G. Sandrone, M. Stave, H. Taylor, G. Thomas, J. van Lenthe, K. Wolinski, A. Wong, Z. Zhang, NWChem 4.0, Pacific Northwest Natl. Laboratory, Richland, Washington 99352, 2000.
[28] A. Klamt, in: P.v.R. Schleyer, N.L. Allinger, T. Clark, J. Gasteiger, P.A. Kollman, H.F. Schaefer III, P.R. Schreiner (Eds.), COSMO and COSMO-RS, Encyclopedia of Computational Chemistry, Vol. 1, Wiley, Chichester, UK, 1998, pp. 604–615.
[29] C. Gonzales, H.B. Schlegel, J. Chem. Phys. 90 (1989) 2154–2161. M.S. Gordon, J.H. Jensen, Acc. Chem. Res. 29 (1996) 536.
[30] M.W. Schmidt, M.S. Gordon, Ann. Rev. Phys. Chem. 49 (1998) 233–266.
[31] M.W. Schmidt, K.K. Baldridge, J.A. Boatz, S.T. Elbert, M.S. Gordon, J.H. Jensen, S. Koseki, N. Matsunaga, K.N. Nguyen, S.J. Su, T.L. Windus, M. Dupuis, J.A. Montgomery, J. Comput. Chem. 14 (1993) 1347–1363.
[32] R.R. Holmes, J.A. Deiters, J. Am. Chem. Soc. 99 (1977) 3318.
[33] MOLDEN: G. Schaftenaar, J.H. Noordik, J. Comput.-Aided Mol. Design 14 (2000) 123–134.
[34] A.E. Reed, L.A. Curtiss, F. Weinhold, Chem. Rev. 88 (1988) 899.
[35] P. Wang, Y. Zhang, R. Glaser, A.E. Reed, P.v.R. Schleyer, A. Streitwieser, J. Am. Chem. Soc. 113 (1991) 55–64.
[36] O.V. Gritsenko, B. Ensing, P.R.T. Schipper, E.J. Baerends, J. Phys. Chem. A 104 (2000) 8558. M. Grüning, O.V. Gritsenko, S.J.A. van Gisbergen, E.J. Baerends, J. Phys. Chem. A 105 (2001) 9211–9218.
[37] T.N. Truong, W.T. Duncan, R.L. Bell, ACS Symp. Ser. 629 (1996) 85. J. Baker, M. Muir, J. Andzelm, A. Scheiner, ACS Symp. Ser. 629 (1996) 342. J. Truhlar, Faraday Discuss. 119 (1998) 362.
[38] B.J. Lynch, P.L. Fast, M. Harris, D.G. Truhlar, J. Phys. Chem. A 104 (2000) 4811–4815. B.J. Lynch, D.G. Truhlar, J. Phys. Chem. A 105 (2001) 2936–2941.
[39] Y. He, J. Gräfenstein, E. Kraka, D. Cremer, Mol. Phys. 98 (2000) 1639–1658. D. Cremer, P.v.R. Schleyer, N.L. Allinger, T. Clark, J. Gasteiger, P.A. Kollman, H.F. Schaefer III, P.R. Schreiner, Encyclopedia of Computational Chemistry Vol. 3 Wiley, Chichester, 1988, p. 615.
[40] A. Dejaegere, X. Liang, M. Karplus, J. Chem. Soc. Faraday Trans. 90 (1994) 1763. S. Bakalova, W. Siebrand, A. Fernandez-Ramos, Z. Smedarchina, D.D. Petkov, J. Phys. Chem. B 106 (2002) 1476.
[41] C. Kötting, W. Sander, J. Am. Chem. Soc. 121 (1999) 8891–8897. J. Kaneti, Helv. Chim. Acta 83 (2000) 836.